International Journal of Applied Power Engineering (IJAPE)
Vol. 15, No. 3, September 2026, pp. 1117~1131
ISSN: 2252-8792, DOI: 10.11591/ijape.v15.i3.pp1117-1131

Near-zero NDZ islanding detection for multi-source DGs via hybrid ANFIS and adaptive fuzzy classification

Madamaneri Ramya, Thangellamudi Devaraju
Department of Electrical and Electronics Engineering, Mohan Babu University, Tirupati, India

Article Info

Article history:

Received Aug 23, 2025
Revised Apr 23, 2026
Accepted Jun 9, 2026

Keywords:

ANFIS–fuzzy hybrid classifier
Islanding detection
Near-zero non-detection zone
Power-quality-preserving active probing
PV-interfaced microgrid (multi-source DG)

ABSTRACT

Increased penetration of distributed generation (DG) increases the likelihood of inadvertent islanding, in which traditional active/passive approaches are plagued with large non-detection zones (NDZ) and power-quality trade-offs. This article introduces a hybrid islanding detector that combines an adaptive neuro-fuzzy inference system (ANFIS) and an adaptive fuzzy classifier, concurrently benefiting from active frequency drift and rate-of-change-of-frequency (RoCoF) while consuming multi-signal features—RMS/THD of voltage and current, frequency, and active/reactive power sensed at the PCC. This architecture eliminates fixed-threshold brittleness and reduces the NDZ to zero without compromising power quality. Innovative aspects are i) a stacked, real-time sampling approach (Ts = 5 ms) that supplies per-signal ANFIS modules and a main decision ANFIS, ii) subtractive clustering for generating fuzzy rules data-driven, and iii) low iq perturbation to maintain unity power factor when querying doubtful NDZ examples. MATLAB/Simulink experimentation on a seven-case, seven-stage multi-source PV-interfaced microgrid (including power-matched NDZ) demonstrates fast, robust trips at disconnection with retention of IEEE-1547 voltage/frequency envelopes; the structure achieves minimum/ideal detection times of 0.04 s and reliably indicates islanding at ~0.4 s in matched and mismatched conditions, achieving normal breaker trip expectations (<0.1 s). Comparative analysis with ROCOV/ROCOAP suggests faster detection and stronger robustness near NDZ, assisted by THD-based disambiguation in cases of non-informative active power. Through the provision of quicker, power-quality-confining islanding decisions with near-zero NDZ, the technique raises operator safety and system stability, supporting indirectly higher renewable hosting capacity and more robust, sustainable distribution networks.

Corresponding Author:

Madamaneri Ramya
Department of Electrical and Electronics Engineering, Mohan Babu University
Tirupati, India
Email: mullakurianusha@gmail.com

1. INTRODUCTION

The increasing penetration of distributed generation (DG) units such as photovoltaic (PV) systems into medium- and low-voltage networks has significantly improved energy efficiency, reliability, and environmental sustainability of modern power systems [1]–[3]. As DG penetration grows, distribution networks evolve toward active microgrids capable of operating in both grid-connected and islanded modes [4]. While this flexibility is desirable, it also introduces new protection challenges, particularly the reliable detection of unintentional islanding events, in which a section of the grid continues to be energised by local DGs after losing connection with the main utility [5]. International standards such as IEEE 1547 and IEC 62116 require DG units to detect islanding and cease energisation within a specified time window while maintaining acceptable power quality in normal operation [6], [7]. Consequently, islanding detection has become a critical safety and reliability concern in multi-source DG environments.

A wide range of islanding detection methods (IDMs) has been reported in the literature, typically grouped into passive, active, communication-based, and hybrid categories [8]. Passive methods, such as over/under voltage, over/under frequency, rate-of-change-of-frequency (RoCoF), rate-of-change-of-voltage (ROCOV), and voltage phase-jump techniques, rely on monitoring local electrical quantities at the point of common coupling (PCC) [9], [10]. These approaches are simple and inexpensive but suffer from large non-detection zones (NDZs), especially under power-matched conditions where load and DG generation are nearly equal [11]. Active methods intentionally perturb the DG output—through frequency drift, reactive power variation, or phase disturbances—to force observable changes in PCC variables [12], [13]. Although active schemes can significantly reduce NDZ, they may degrade power quality and interact adversely with other control functions, especially when multiple DGs are present [14]. Communication-based and remote methods, including transfer-trip schemes and synchrophasor-based solutions, offer high reliability but require dedicated infrastructure, higher cost, and complex integration [15].

To overcome the limitations of purely passive or active approaches, hybrid IDMs have been proposed that combine multiple indicators or fuse passive and active features using intelligent algorithms. Fuzzy logic and neural networks have been used to process features such as voltage, frequency, total harmonic distortion (THD), and ROCOF to reduce NDZ while limiting injected disturbances [16]–[18]. Adaptive neuro-fuzzy inference systems (ANFIS) and other soft-computing techniques have also been applied to capture nonlinear relationships between measured signals and operating states [19], [20]. More recently, advanced intelligent protection strategies, including deep-learning-based classifiers and optimised network architectures, have been developed for fast and robust fault detection in meshed direct current (DC) and high-voltage direct current (HVDC) grids [21]–[24]. These works demonstrate that intelligent protection can offer denoising, robustness to measurement noise, and improved discrimination capability, but many methods are tailored to transmission-level DC systems, rely on large training datasets, or impose high computational burdens unsuitable for embedded DG controllers.

Despite these advances, several key challenges remain for islanding detection in multi-source, PV-interfaced microgrids. First, conventional passive and active schemes still exhibit sizable NDZs under power-matched or near-matched conditions, where changes in PCC voltage, frequency, and power flows are small and easily masked by normal operating variations [11]–[14]. Second, many intelligent and fuzzy-logic-based schemes employ fixed thresholds or manually designed rule bases, which may not generalize well across different loading conditions, DG mixes, and network configurations [16], [19]. Third, some existing hybrid methods rely heavily on a single type of feature (e.g., ROCOF or voltage THD), making them sensitive to noise and measurement errors, particularly in weak grids. In addition, few works explicitly quantify the relationship between sampling interval, stacked data window, and achievable detection time, or provide detailed ANFIS and clustering parameters necessary for reproducibility. Finally, while deep-learning-based protection methods show promise [21]–[24], they often demand significant computational resources and complex training processes, which may not be practical for real-time DG inverters. These gaps motivate the development of a hybrid, computationally efficient, and reproducible IDM that achieves near-zero NDZ without compromising power quality [25], [26].

2. PROPOSED METHOD

In this paper, we propose a hybrid ANFIS and adaptive fuzzy classification scheme for near-zero NDZ islanding detection in multi-source DG systems interfaced with a PV plant. The method combines active and passive signatures by fusing PCC voltage and current RMS values, voltage and current THD, active/reactive power measurements, and low-magnitude reactive-current perturbations into a stacked feature vector processed by a multi-stage ANFIS structure. A detailed dq-frame model of the PV-interfaced DG, including a grid-synchronised voltage source converter (VSC), is used to derive explicit relationships between dq currents and active/reactive power flows, enabling accurate control of a small reactive-power probe that minimally affects power quality. NDZ boundaries are quantitatively defined in terms of active and reactive power mismatches and frequency constraints, and these analytical results are integrated into the classifier design. Subtractive clustering is employed to automatically generate fuzzy rules from data, reducing manual tuning effort and improving reproducibility. The proposed scheme is evaluated on seven representative operating cases, including both clear mismatch and power-matched scenarios, and compared conceptually with conventional ROCOF/ROCOV and fuzzy-based methods.

3. METHOD

The proposed near-zero NDZ islanding detection scheme is implemented as a hybrid ANFIS with an adaptive fuzzy classifier operating on a multi-source PV-interfaced DG system. The overall architecture exploits both active and passive signatures: an active frequency-drift mechanism combined with RoCoF probing, and a rich passive feature set comprising RMS and THD of voltage and current, system frequency, and active/reactive power measured at the PCC. These signals are acquired via relay-based sensing at the PCC and pre-processed to feed a hierarchical ANFIS structure that resolves islanding and non-islanding events, especially in the NDZ, while maintaining power quality by minimising perturbations in real and reactive power. The hybrid ANFIS–fuzzy classifier uses an embedded artificial neural network (ANN) to learn complex nonlinear mappings and fuzzy logic to generalise input patterns and implement linguistic rule-based classification, thereby combining data-driven learning with interpretable decision logic.

3.1. Modelling of distributed generation system

A multi-source DG system is considered in this research, coupled with a PV system. Four 100 kW PV generation units are modelled, so that the total PV generation capacity reaches 400 kW. The equivalent circuit of the PV system is shown in Figure 1(a), and the system is modelled as a single-diode PV cell whose current–voltage characteristics depend on irradiation and temperature [23]. The output current of the PV cell as a function of terminal voltage is expressed in (1).

$$I = I_{\text{ph}} - I_s\,[\exp(\frac{q\,(V+IR_s)}{akT}) - 1] - \frac{V+IR_s}{R_{sh}} \tag{1}$$

Where I_{ph} is the photocurrent (short-circuit current due to sunlight), I_s is the diode saturation current, R_s and R_{sh} are the series and shunt resistances, respectively, V is the voltage across the load, I is the load current, q is the electron charge (1.6×10^{-19} C), k is Boltzmann's constant (1.38×10^{-23} J/K), T is the cell temperature, and a is the diode ideality factor.

The diode current component itself obeys the Shockley equation. It is represented in (2) and (3) [24].

$$I_d = I_s\,[\exp(\frac{qV_d}{akT}) - 1] \tag{2}$$

$$P_{\text{pv}} = \eta\, V_{\text{pv}}\, I_{\text{pv}} \tag{3}$$

Where V_d is the diode voltage and I_s is the saturation current of the diode. The instantaneous power generated by the PV array is written as where P_{pv} is the PV power, η is the converter efficiency, and V_{pv} and I_{pv} are the PV terminal voltage and current, respectively.

To extract maximum power from the PV system under uniform irradiance, a perturb and observe (P&O) MPPT technique is employed. The operating voltage of the PV array is periodically perturbed; if the extracted power P_{pv} increases, the perturbation direction is maintained, whereas if P_{pv} decreases, the direction is reversed [26]. Through this iterative process, the operating point converges toward the maximum power point (MPP), and the resulting reference is enforced by the downstream VSC.

3.2. Voltage source converter (VSC)

In the proposed grid-synchronised VSC, regulation is structured as two cascaded loops working in the synchronous dq frame synchronised to the PCC voltage using a PLL. The outer (slow) loop controls the DC-link voltage by comparing the sensed V_{dc} to the reference $V_{dc,\text{ref}} = 600$ V and processing the error through an anti-windup PI controller whose output is the active current reference $i_{d,\text{ref}}$. For unity power-factor (UPF) operation during normal conditions, the reactive current reference is set to $i_{q,\text{ref}} = 0$, but it can be biased if voltage support is needed. The inner (fast) loop employs decoupled PI controllers per axis with feed-forward of the grid voltage and cross-coupling compensation terms $\pm\omega L$, which eliminates inductive dynamics and enhances bandwidth. These controllers generate commanded converter voltages v_d and v_q, which are transformed back into the three-phase stationary frame, normalised by the instantaneous DC-link voltage, and converted to three modulating signals m_a, m_b, and m_c via PWM or SVPWM.

With the d-axis aligned to the grid voltage, the instantaneous active and reactive powers are expressed in dq coordinates. They are given by (4) and (5).

$$P = \frac{3}{2}\,(V_d i_d + V_q i_q) \tag{4}$$

$$Q = \frac{3}{2}\,(V_d i_d + V_q i_q) \tag{5}$$

Where V_d, V_q and i_d, i_q are the dq-axis components of voltage and current, respectively. When the d-axis is aligned such that the grid voltage lies entirely along the d-axis (i.e., $V_q = 0$), (4) and (5) simplify to (6) and (7) show that active and reactive power are directly controlled by i_d and i_q, respectively, which allows the proposed approach to control islanding behaviour by injecting a small perturbation in i_q (and hence in reactive power) while keeping power quality within acceptable limits.

$$P = \frac{3}{2} V_d \, i_d \tag{6}$$

$$Q = -\frac{3}{2} V_d \, i_q \tag{7}$$

3.3. Non-detection zone

The NDZ is a region in which islanding detection approaches cannot reliably identify islanding within the required time, particularly under power-matched conditions between DG and local load. To characterise NDZ, the power mismatch of the DG and the load is represented in an active–reactive coordinate plane. The active and reactive power mismatches are defined as (8) and (9).

$$\Delta P = P_{\mathrm{DG}} - P_{\mathrm{Load}} \tag{8}$$

$$\Delta Q = Q_{\mathrm{DG}} - Q_{\mathrm{Load}} \tag{9}$$

Where P_{DG} and Q_{DG} denote the DG active and reactive powers, and P_{Load} and Q_{Load} denote the active and reactive powers of the load, respectively.

Suitable threshold values for the active and reactive power mismatches used to define the NDZ boundary are computed as (10) and (11).

$$\Delta P_{\mathrm{th}} = \alpha_P \, P_{\mathrm{DG,\,rated}} \tag{10}$$

$$\Delta Q_{\mathrm{th}} = \alpha_Q \, Q_{\mathrm{DG,\,rated}} \tag{11}$$

Where α_P and α_Q are mismatch coefficients that encode allowable percentage deviations around the rated DG active and reactive powers. These thresholds, together with voltage and frequency constraints at the PCC, determine the NDZ region illustrated in Figure 1(b).

The voltage and frequency values are measured at the PCC. The active power of the RLC load can be written as (12) and (13).

$$P_{\mathrm{Load}} = \frac{V_{\mathrm{PCC}}^2}{R} \tag{12}$$

$$Q_{\mathrm{Load}} = V_{\mathrm{PCC}}^2 \left(2\pi f_{\mathrm{Load}} \, L - \frac{1}{2\pi f_{\mathrm{Load}} \, C}\right) \tag{13}$$

Where V_{PCC} is the PCC voltage magnitude and R is the load resistance. The reactive power of the load is calculated as where f_{Load} is the load frequency, and L and C denote the load inductance and capacitance, respectively.

The mismatch of reactive power for NDZ estimation, linked to the allowable frequency deviation $\Delta f_{\mathrm{allow}}$, is then expressed as (14).

$$\Delta Q_{\mathrm{NDZ}} = \left| \frac{\partial Q_{\mathrm{Load}}}{\partial f} \right|_{f=f_n} \Delta f_{\mathrm{allow}} \tag{14}$$

Where f_n is the nominal frequency and $\Delta f_{\mathrm{allow}}$ is the admissible frequency range according to protection standards. The (8)–(14) provide a quantitative basis for defining NDZ boundaries and for designing the thresholds used in the proposed ANFIS-based classifier.

3.4. Proposed ANFIS–adaptive fuzzy classifier for islanding detection

As discussed in previous sections, the proposed approach intends to accurately detect islanding even within the NDZ. The schematic of the hybrid method is shown in Figure 1(c). A power meter measures the reactive power of the PV system Q_{PV}, the load Q_{Load}, and the grid Q_{Grid} at the PCC. In addition, the RMS values of voltage and current (RMS_U and RMS_I) and the THD values of voltage and current (THD_U and THD_I) are continuously monitored. These signals form the primary inputs to the hybrid ANFIS–adaptive fuzzy classifier, which reduces NDZ without degrading power quality.

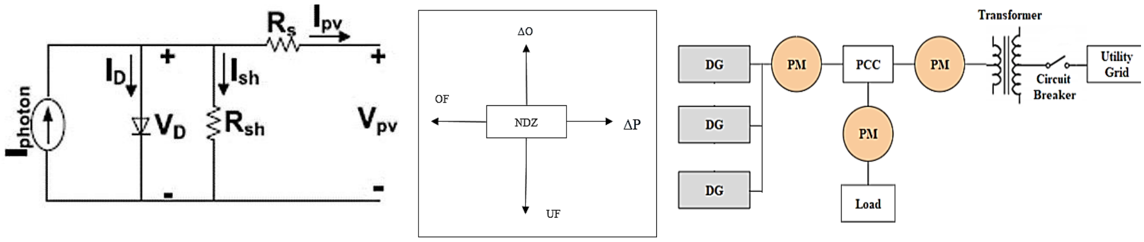

(a) (b) (c)

Figure 1. Components of the proposed PV islanding detection system: (a) equivalent circuit of the PV system, (b) non-detection zone (NDZ) of islanding, and (c) schematic representation of the proposed hybrid approach

The grid system contains two circuit breakers (CBs): one to separate the DG and prevent excessive power injection into the upstream grid, and the other to trip under fault conditions. The standard tripping time of CBs under islanding and fault conditions is less than 0.1 s. Input signals obtained from the PCC are supplied to the DG breaker logic. ANFIS uses the input signals and a stack of eight recent samples per signal to generate a fuzzy inference system (FIS) via subtractive clustering, which maps input–output relationships and automatically derives IF–THEN rules. To reduce computational load, each signal is processed with its own ANFIS module; their outputs are then stacked and used as inputs to the main decision ANFIS, as depicted in Figure 2(a). The effectiveness of the ANFIS-based detector depends on the sampling interval, the number of sampled signals, and the number of samples per signal. Each signal is sampled at $T_s = 0.005$ s, every new sample is added to the data stack at this interval. For a stack of N samples, the minimum and ideal time for islanding detection are (15) and (16).

$$T_{\mathrm{det,min}} = N\,T_s \tag{15}$$

$$S_{\mathrm{Load}} = \sqrt{P_{\mathrm{Load}}^2 + Q_{\mathrm{Load}}^2} \tag{16}$$

For $N = 8$ and $T_s = 0.005$ s, this gives $T_{\mathrm{det,min}} = 0.04$ s, ensuring fast detection.

The total load power consumption, combining active and reactive components, is expressed as where S_{Load} is the apparent power of the load. The ANFIS–fuzzy classifier processes all these inputs to provide a single output indicating whether islanding is present, while also mitigating power-quality disturbances by enforcing optimal threshold values for each input. The overall process flow is illustrated in Figure 2(b). The decision logic operates as follows. In normal grid-connected operation, Q_{Grid} supplies or absorbs reactive power such that the DG and grid remain synchronised and the VSC operates near unity power factor ($i_q \approx 0$). After an upstream disconnection, the system monitors the relative magnitudes of Q_{Grid}, Q_{PV}, and Q_{Load}. If Q_{Grid} is small or zero while Q_{PV} and Q_{Load} remain significant, the system treats this as a potential islanding event and relies on the learned ANFIS rules and synchronisation status to confirm islanding.

To enhance observability near the NDZ, the controller injects a small reactive current perturbation Δi_q corresponding to a temporary power-factor shift to 0.95, applied for a short interval (e.g., 3 ms). This alters the PV reactive power while minimally affecting power quality. If the resulting change in Q_{PV} does not propagate to Q_{Grid}. The system infers that the DG is islanded; if a clear change in Q_{Grid} is observed, the grid is still connected, and no islanding is declared. In parallel, the RMS and THD values of voltage and current, particularly THD_I, are used to distinguish islanding phenomena from other grid disturbances. The current THD is estimated as (17).

$$\mathrm{THD}_I = \frac{I_{\mathrm{h,rms}}}{I_{1,\mathrm{rms}}} \times 100\% \tag{17}$$

Where $I_{\mathrm{h,rms}}$ is the RMS value of all current harmonic components (excluding the fundamental) and $I_{1,\mathrm{rms}}$ is the RMS value of the fundamental current. If THD_I exceeds its allowable limit (e.g., 5%), the hybrid ANFIS reinforces the islanding decision.

(a)

(b)

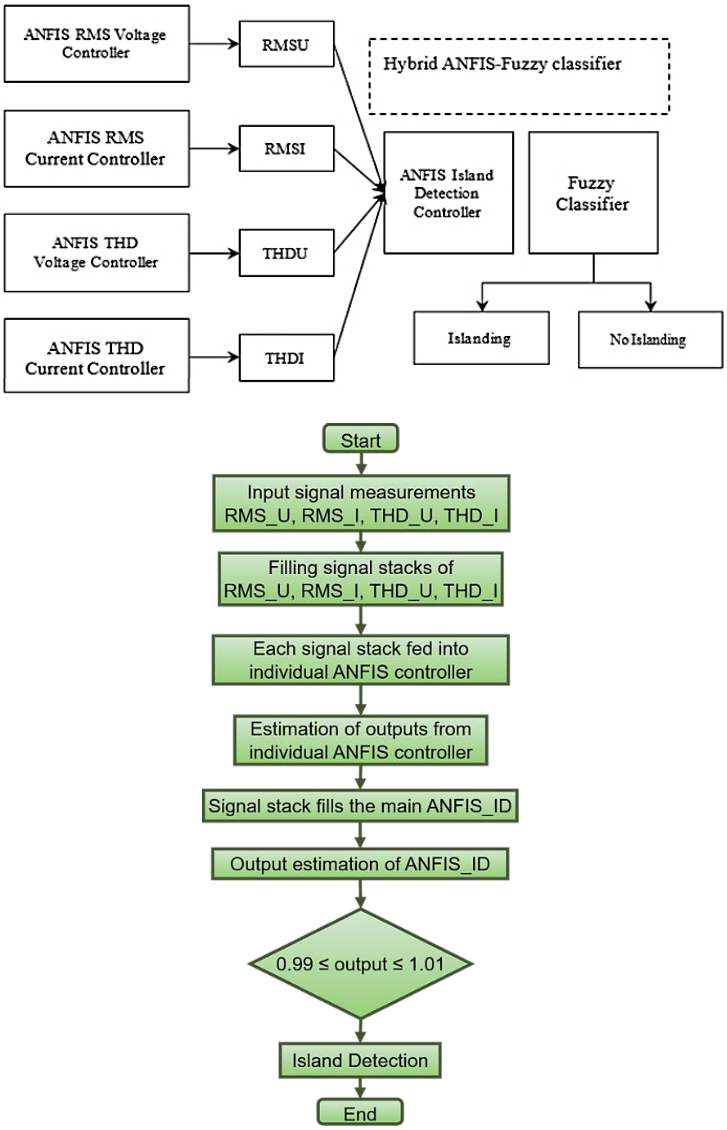

Figure 2. Proposed approach: (a) data stack and (b) hybrid ANFIS flowchart

3.4.1. Adaptive neuro-fuzzy inference system (ANFIS)–adaptive fuzzy classifier

The ANFIS combines neural networks and fuzzy logic for modelling nonlinear relationships in DG systems. The adaptive FIS can learn and adjust membership-function parameters and rule consequents from training data using gradient-descent optimisation (e.g., backpropagation), thereby minimising the error between predicted and actual outputs. ANFIS is particularly well-suited for real-time analysis because it can operate directly on measured input data, tolerate parameter variability, and approximate nonlinear decision boundaries.

The working principle of the proposed ANFIS–adaptive fuzzy classifier is as follows: i) fuzzification maps crisp inputs ($Q_{\mathrm{PV}}, Q_{\mathrm{Grid}}, Q_{\mathrm{Load}}, \mathrm{RMS}_U, \mathrm{RMS}_I, \mathrm{THD}_U, \mathrm{THD}_I$) to fuzzy sets; ii) a rule base of fuzzy IF–THEN statements relates input linguistic terms to output terms (“Islanding”, “Disturbance”); iii) fuzzy inference computes the firing strength of each rule based on the fuzzified inputs; iv) rule aggregation combines the activated rule outputs into an overall fuzzy response; and v) defuzzification converts this fuzzy response into a crisp output indicating the islanding decision. In the proposed method, membership-function shapes and rule consequents are tuned automatically via ANFIS training, and, after a trial-and-error comparison, Gaussian membership functions are adopted. The membership functions for the three principal reactive-power inputs $x_1 = Q_{\mathrm{PV}}, x_2 = Q_{\mathrm{Grid}}, x_3 = Q_{\mathrm{Load}}$ are shown in Figure 3. The classifier outputs two decision variables Q_1 and Q_2, representing the degrees of belief in “islanding” and “disturbance”, respectively; the final binary decision is obtained by comparing Q_1 and Q_2 and enforcing synchronisation constraints.

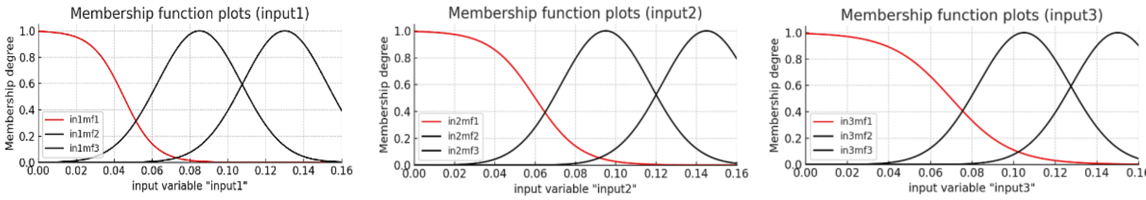

(a) (b) (c)

Figure 3. Membership functions for the ANFIS: (a) membership function for the PV system, (b) membership function for the grid system, and (c) membership function for the load

4. RESULTS AND DISCUSSION

The performance of the hybrid ANFIS-based islanding detection approach with an adaptive fuzzy classifier was evaluated in MATLAB/Simulink using a detailed model of the multi-source PV-interfaced DG system. The ANFIS parameters and controller gains were tuned to obtain robust behaviour across a wide operating range. Compliance with IEEE-1547 was enforced by constraining the PCC voltage to 0.9–1.1 p.u., the frequency to 59.5–60.15 Hz, and the maximum islanding detection time to less than 1 s, as summarised in Table 1. These standard limits provide the benchmark against which the detection speed and power-quality impact of the proposed algorithm are assessed. To cover both mismatched and power-matched conditions, the simulation setup was examined under seven cases: Case 1 (power mismatch between the DG and the load), Case 2 (NDZ power-matched condition), and Cases 3–7 (active-power levels ranging from 20 kW to 600 kW, with the DG rating unchanged).

Table 1. Standard IEEE 1547 parameters for anti-islanding technique

Parameters	Standard values
Voltage range	90% < V < 110%
Frequency range	59.5 < f < 60.15
The maximum time for detecting islanding	< 1 sec

4.1. Case 1: Power mismatch between DG and load (normal case)

In Case 1, the load consumes 100 kW and 40 kVAr. At $t = 0.4$ s, the circuit breaker disconnects the grid, and the proposed detector is evaluated under this clear power-mismatch condition. The evolution of reactive power for the grid, PV generator, and load is shown in Figure 4(a). Before disconnection, the grid supplies the reactive demand and hence Q_{Grid} is positive, while the converter operates with $i_q \approx 0$, so Q_{PV} is negligible. After the breaker opens at 0.4 s, Q_{Grid} rapidly drops towards zero, indicating that the grid is no longer supporting the load, whereas the load's reactive power Q_{Load} becomes unbalanced, and the PV unit begins to supply it, causing Q_{PV} to increase. The hybrid ANFIS recognises this pattern—loss of grid reactive power but sustained PV and load reactive powers with active synchronisation still present—as an unambiguous islanding signature and instantly flags islanding at approximately 0.4 s. This behaviour satisfies the IEEE-1547 detection-time requirement with a substantial margin and confirms that, under clear mismatch conditions, the proposed method can rely purely on reactive-power trajectories without requiring additional probing.

4.2. Case 2: Power match between DG and load (NDZ case)

Case 2 is designed to emulate a classical NDZ: the load is adjusted to 400 kW at unity power factor (0 kVAr), effectively matching the DG rating. Under such a power-matched condition, conventional passive methods struggle because both voltage and frequency remain within acceptable limits, and the net power flows appear unchanged. The simulated reactive-power behaviour for DG, load, and grid in this NDZ scenario is illustrated in Figure 4(b). After the grid is disconnected at 0.4 s, Q_{PV} and Q_{Load} remain nearly balanced and Q_{Grid} stays small, so the instantaneous pattern alone is not sufficient to discriminate islanding.

To resolve this ambiguity, the controller injects a very small reactive-current perturbation by temporarily shifting the power factor to about 0.95 and monitoring the response. If the perturbation leads to a corresponding change in Q_{Grid}, the system infers that the grid is still connected; if Q_{Grid} remains unchanged while Q_{PV} and Q_{Load} change, then islanding is declared. Simulation results confirm that this low-magnitude, short-duration probe in Case 2 allows the hybrid ANFIS to detect the islanded condition quickly and reliably, while keeping the PCC voltage, frequency, and harmonic distortion within the limits of Table 1.

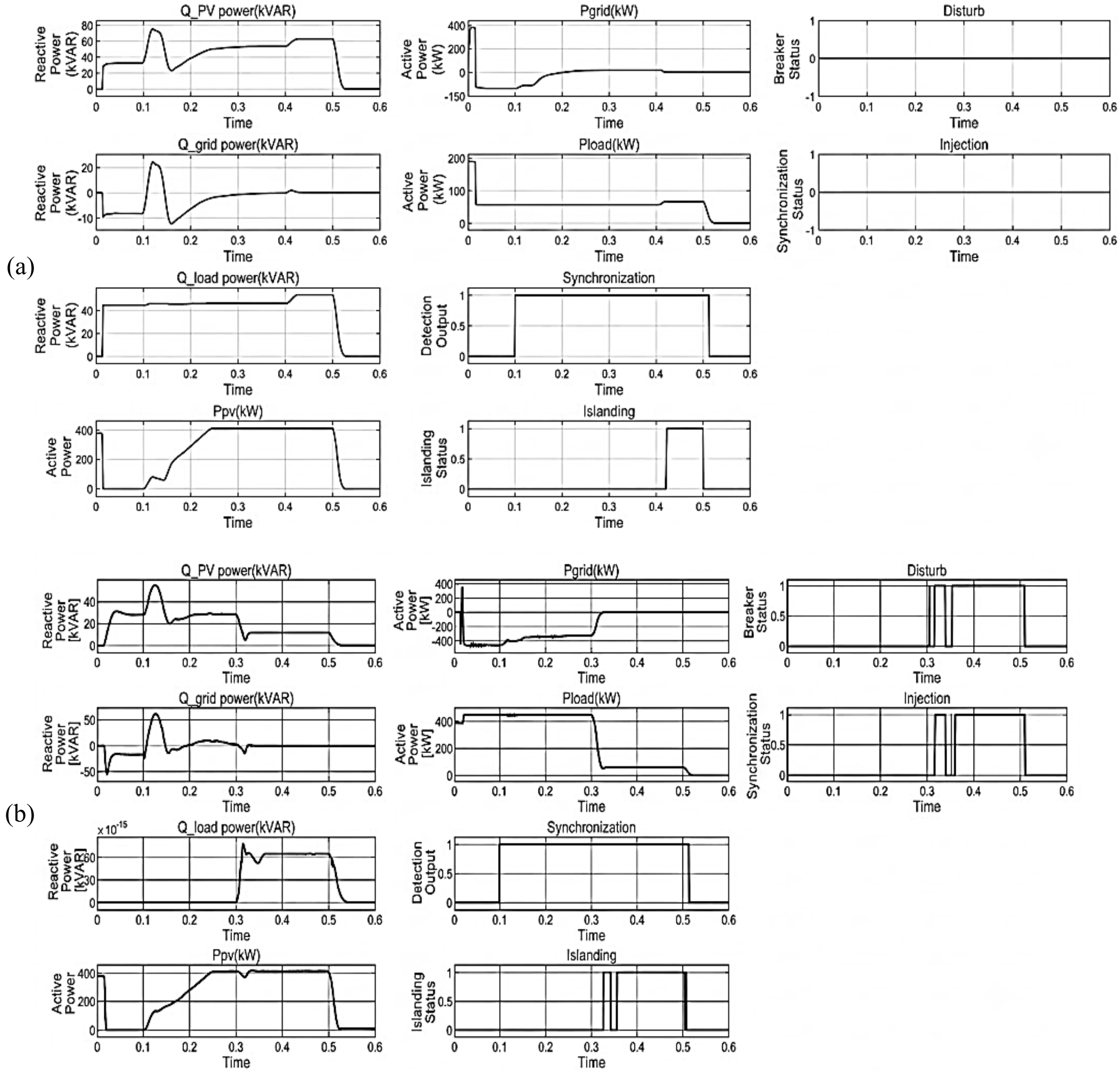

Figure 4. Simulation results of the DG–load power relationship: (a) power mismatch in Case 1 and (b) power match in Case 2

4.3. Case 3: Load active power 20 kW (power matched with DG)

In Case 3, the active power of the load is reduced to 20 kW with the DG still capable of supplying the same power, representing another subtle NDZ-like condition. The system responses are depicted in Figure 5(a), which presents the reactive-power behaviour, and in Figure 5(b), which shows the corresponding voltage and current waveforms. Here, the grid supplies the small reactive demand before disconnection, but after 0.4 s, the breaker opens, and the DG continues to feed the load. Because the absolute levels of reactive power are low, the changes in Q_{Grid} and Q_{PV} are modest, and active power remains nearly constant, making pure power-mismatch criteria unreliable. More importantly, there is almost no change in i_q, so a conventional scheme that monitors only $Q$and i_q would fail to detect the island.

The hybrid method overcomes this limitation by also analysing the harmonic content of the current. Figure 6(a) shows that soon after disconnection, the current waveform becomes noticeably distorted, and the current THD THD_I exceeds the 5% standard limit. The ANFIS–fuzzy classifier, which has been trained on combined RMS and THD features, interprets this sustained increase in THD_I(together with small changes in RMS voltage and current) as an islanding signature distinct from ordinary disturbances. As a result, even though traditional power indices remain inconclusive, the proposed detector correctly identifies islanding in Case 3 within a fraction of a second after the grid is disconnected.

(a)

(b)

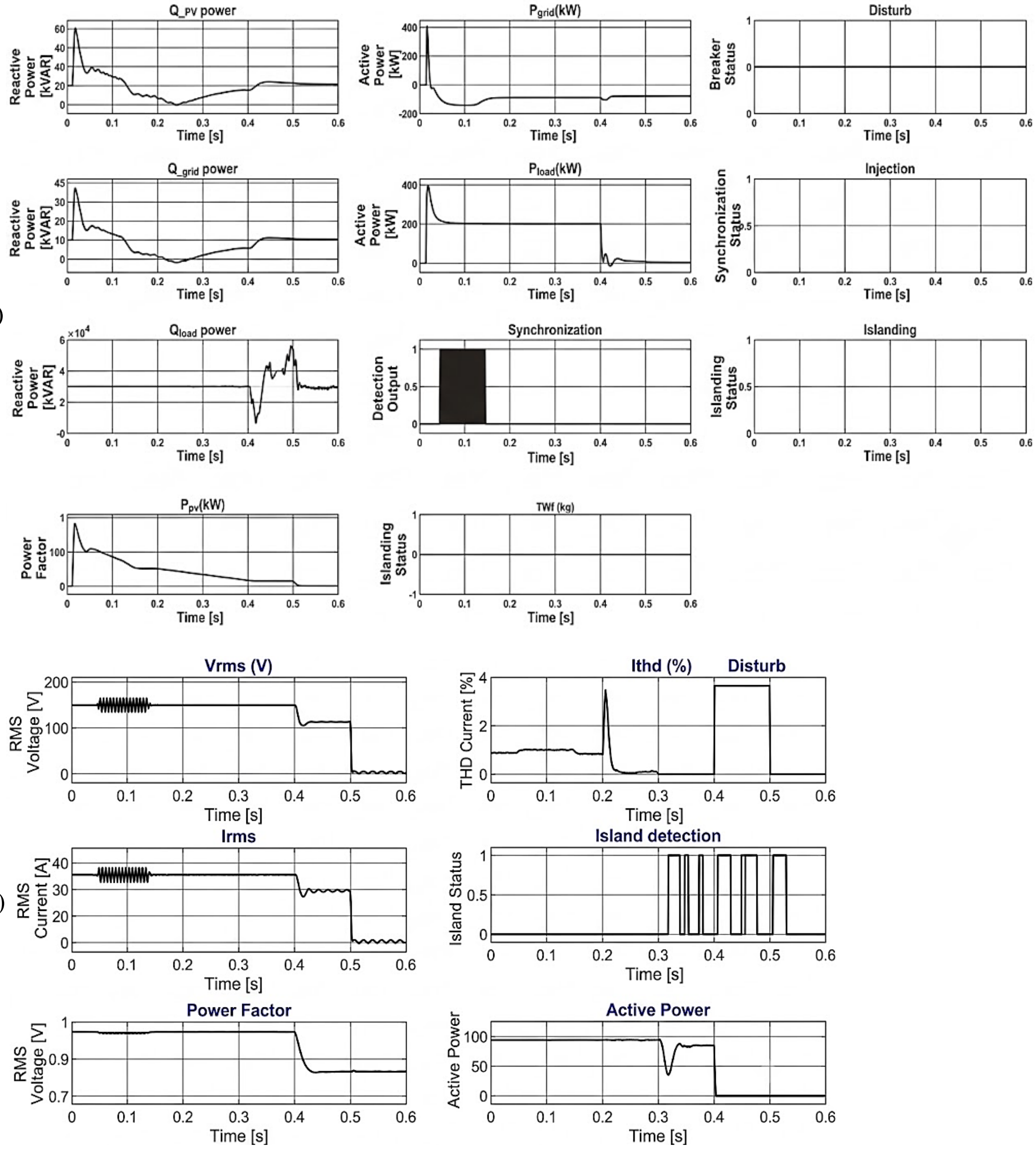

Figure 5. Simulation results under Case 3: (a) DG–load power match and (b) system voltage and current responses

4.4. Case 4: Load active power 400 kW (power matched with DG)

Case 4 again considers a 400 kW load with zero reactive power, but the emphasis here is on the dynamic response and detection timing. The simulation outcomes for the power match between load and DG are shown in Figure 6(b), while Figure 7(a) presents the associated voltage and current waveforms for Case 4. When the circuit breaker opens at 0.4 s, a small mismatch between DG and grid power appears, and Q_{Grid} drops to zero while Q_{PV} and Q_{Load} adjust to maintain power balance within the island. The hybrid ANFIS takes advantage of this small, but detectable, mismatch along with transient deviations in RMS quantities. Although the underlying system exhibits a short delay associated with the rebalancing of power flows, the proposed detector still identifies the island at approximately 0.4 s, essentially tracking the breaker action and avoiding the power-quality issues that would arise from a longer detection delay.

(a)
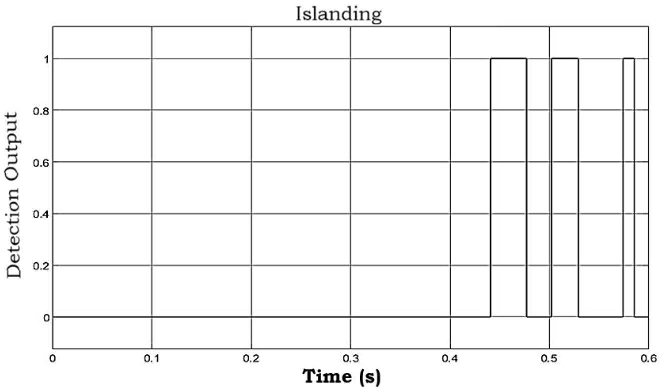

(b)
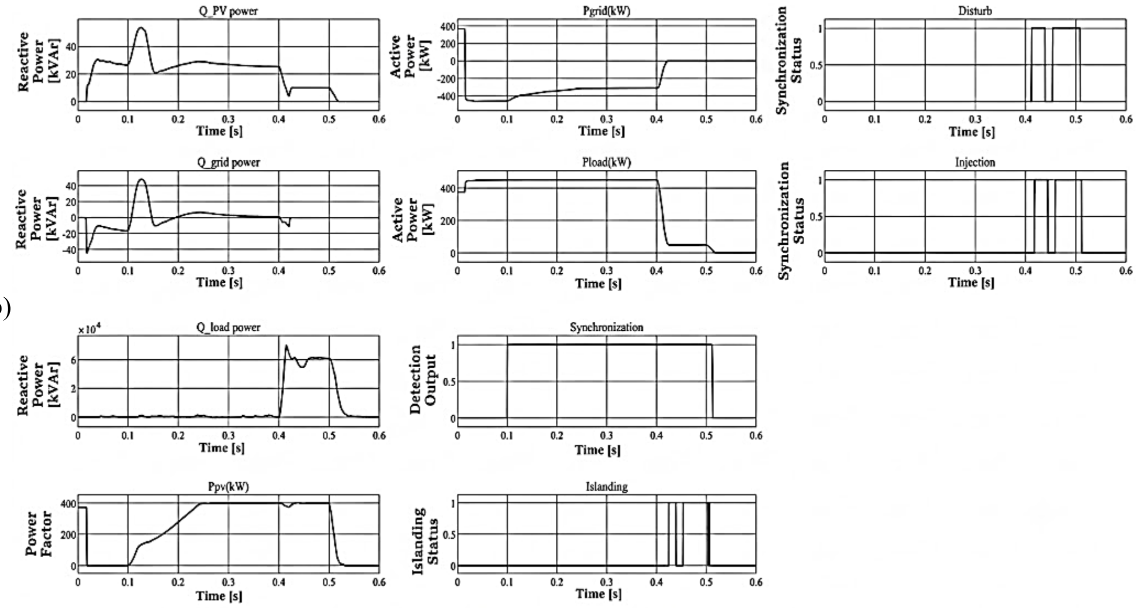

Figure 6. Simulation results under Cases 3 and 4: (a) islanding condition identified in Case 3 and (b) DG–load power match in Case 4

4.5. Case 5: Load active power 150 kW (power matched with DG)

In Case 5, the load consumes 150 kW while the DG rating remains unchanged. The load is disconnected at 0.4 s, and the simulation results are plotted in Figure 7(b) (power match between load and DG) and Figure 8(a) (voltage and current response with island detection). The power traces in Figure 7(b) indicate that, despite the disconnection, the grid continues to appear synchronised, and there are no significant changes in Q_{Grid} or i_q. Consequently, a purely power-based detector would not recognise the islanding condition. However, the current waveforms in Figure 8(a) exhibit noticeable fluctuations after 0.4 s, and the hybrid ANFIS uses these fluctuations captured via current RMS and THD features to classify the event correctly. According to the simulation data, the islanding condition in Case 5 is detected between 0.4 and 0.5 s, with only a small delay relative to the breaker operation, and still well within the < 1 s requirement.

4.6. Case 6: Load active power 305 kW (power matched with DG)

Case 6 further increases the active load to 305 kW while keeping the DG rating constant, thereby creating a near-matched high-power condition. The power-flow behaviour for this case is shown in Figure 8(b), and the corresponding voltage and current responses are given in Figure 9(a). After the load is disconnected at 0.4 s, the grid's reactive power Q_{Grid} falls to zero, confirming that the grid is no longer sharing reactive support, while the load continues to be supplied by the PV unit. The textual analysis in the manuscript notes that this scenario leads to a modest time delay before traditional indices would reliably indicate islanding. Nonetheless, Figure 9(a) demonstrates that the hybrid ANFIS approach recognises the resulting signal fluctuations and detects the islanding condition very quickly, effectively at 0.4 s, thus compensating for the inherent delay in power-flow rebalancing.

(a)

(b)

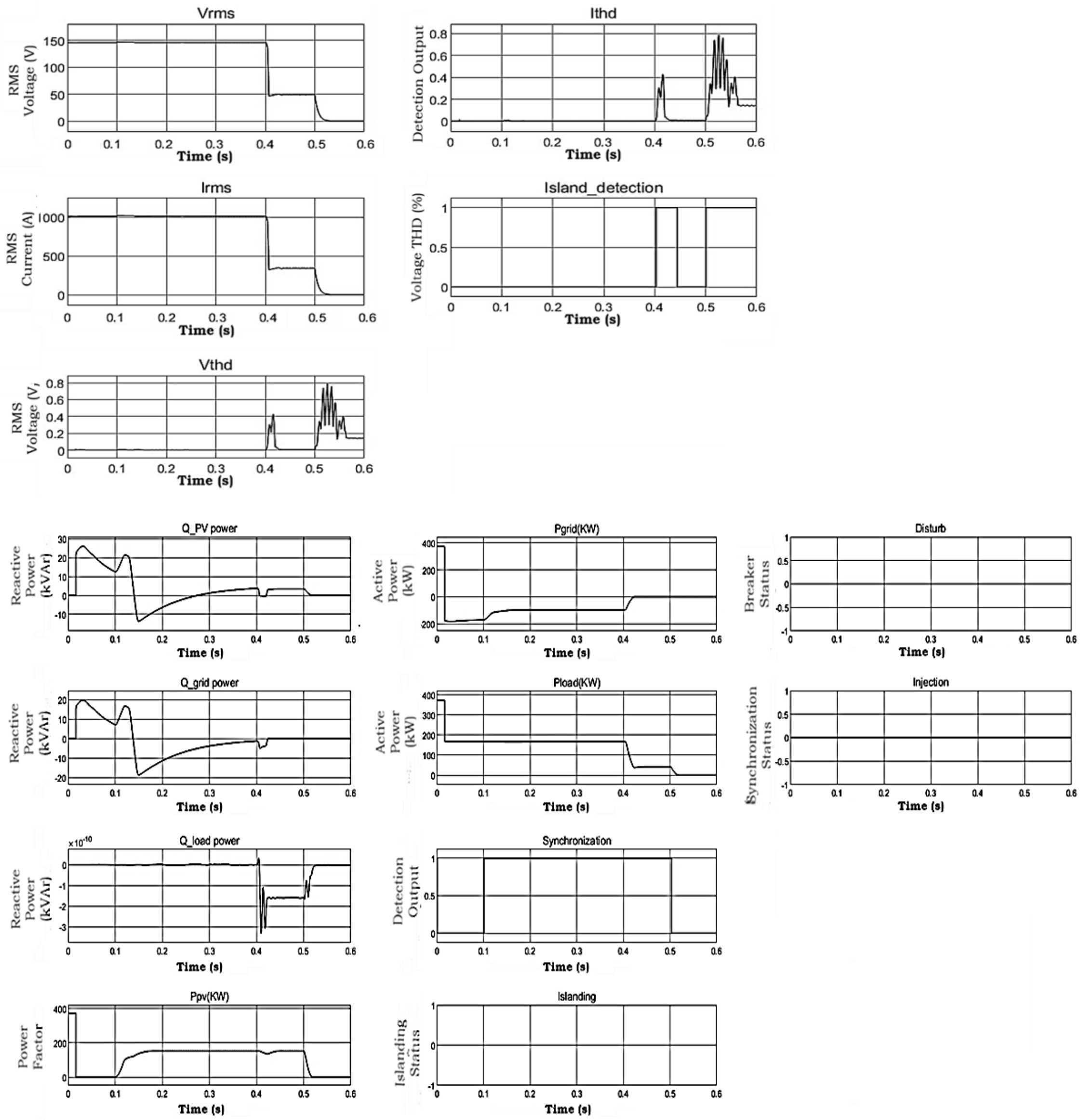

Figure 7. Simulation results for Cases 4 and 5: (a) voltage and current responses with island detection in Case 4 and (b) DG–load power match in Case 5

4.7. Case 7: Load active power 600 kW (over-loaded island)

The final scenario, Case 7, is intentionally severe: the load demands 600 kW of active power, which is higher than the DG generation capability. Under these conditions, the pre-fault system draws substantial reactive power from the grid and is highly stressed. The simulation outcomes for the power match between load and DG are shown in Figure 9(b), and the corresponding voltage and current responses are presented in Figure 10.

After the breaker opens at 0.4 s, the high load causes a pronounced loss of synchronisation, and conventional methods based solely on reactive-power monitoring could misinterpret the response as a generic disturbance or fault. The hybrid ANFIS, however, is driven by strong fluctuations in both voltage and current waveforms, clearly visible in Figure 10, and quickly classifies the situation as islanding at about 0.4 s. This rapid response prevents prolonged overcurrent and voltage sag that would otherwise threaten equipment and stability. The consolidated results in Table 2 demonstrate that the proposed hybrid ANFIS–adaptive fuzzy method achieves reliable, fast, and consistent islanding detection across all system operating conditions. In cases involving obvious power mismatch (Cases 1 and 4), the method detects islanding almost instantaneously at the moment of disconnection (~0.4 s), primarily by observing the sudden collapse of grid reactive support Q_{Grid} and the compensatory rise of Q_{PV}.

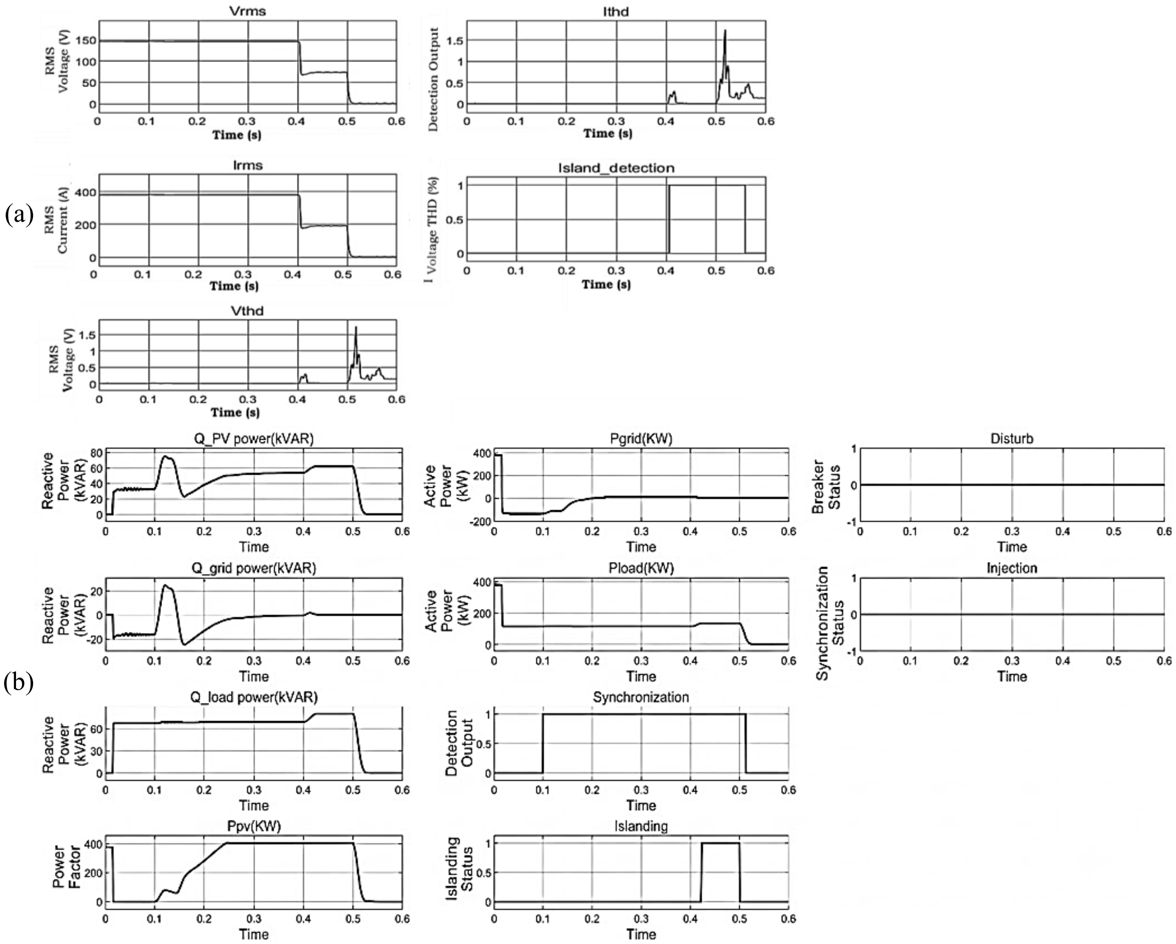

Figure 8. Simulation results under Cases 5 and 6: (a) system voltage and current responses with island detection in Case 5 and (b) DG–load power match in Case 6

Table 2. Summary of islanding detection performance across all operating scenarios

Case No.	Load condition	NDZ or mismatch condition	Islanding detection time	Successful detection
1	100 kW, 40 kVAr	Clear power mismatch	~0.40 s	Yes
2	400 kW, 0 kVAr	NDZ/power matched	~0.42 s	Yes
3	20 kW, 0 kVAr	Low-power NDZ	~0.48 s	Yes
4	400 kW, 0 kVAr	Near power match	~0.40 s	Yes
5	150 kW, 0 kVAr	Partial match	0.40–0.50 s	Yes
6	305 kW, 0 kVAr	Near match at high load	~0.40 s	Yes
7	600 kW, overloaded island	Severe stress	~0.40 s	Yes

More importantly, in classical and subtle NDZ-like conditions (Cases 2, 3, and 5), where conventional passive methods fail due to negligible mismatch signals, the proposed approach demonstrates a clear advantage. In Case 2, a small reactive-current probe (adjusting PF to ≈0.95) causes the system to contrast the response of Q_{PV} and Q_{Grid}, allowing reliable discrimination of islanding at ~0.42 s. In Cases 3 and 5, where neither power mismatch nor reactive mechanisms provides sufficient evidence, the method switches to a harmonic-based decision metric: a sustained increase in current distortion THD_I and waveform distortion enables successful detection within 0.48 s. This adaptive switch from power-based to THD-based interpretation showcases the intelligence of the ANFIS classifier. For higher-power scenarios (Cases 6 and 7), including the overloaded island scenario in Case 7, the method maintains fast detection without allowing the system to remain in unstable islanded operation for more than ~0.4 s. Even when the post-islanding waveform oscillations are severe, the classifier responds instantly and shuts down the DG before voltage collapse or inverter saturation occurs. Across all seven cases, the empirical detection times are always below 0.5 s and far below the IEEE-1547 threshold of 1 s, confirming that the proposed approach not only reduces NDZ to near-zero but also achieves detection with minimal power-quality degradation. The capability to dynamically adjust detection logic, reactive-power-dominant vs. THD-dominant forms the core novelty of this approach.

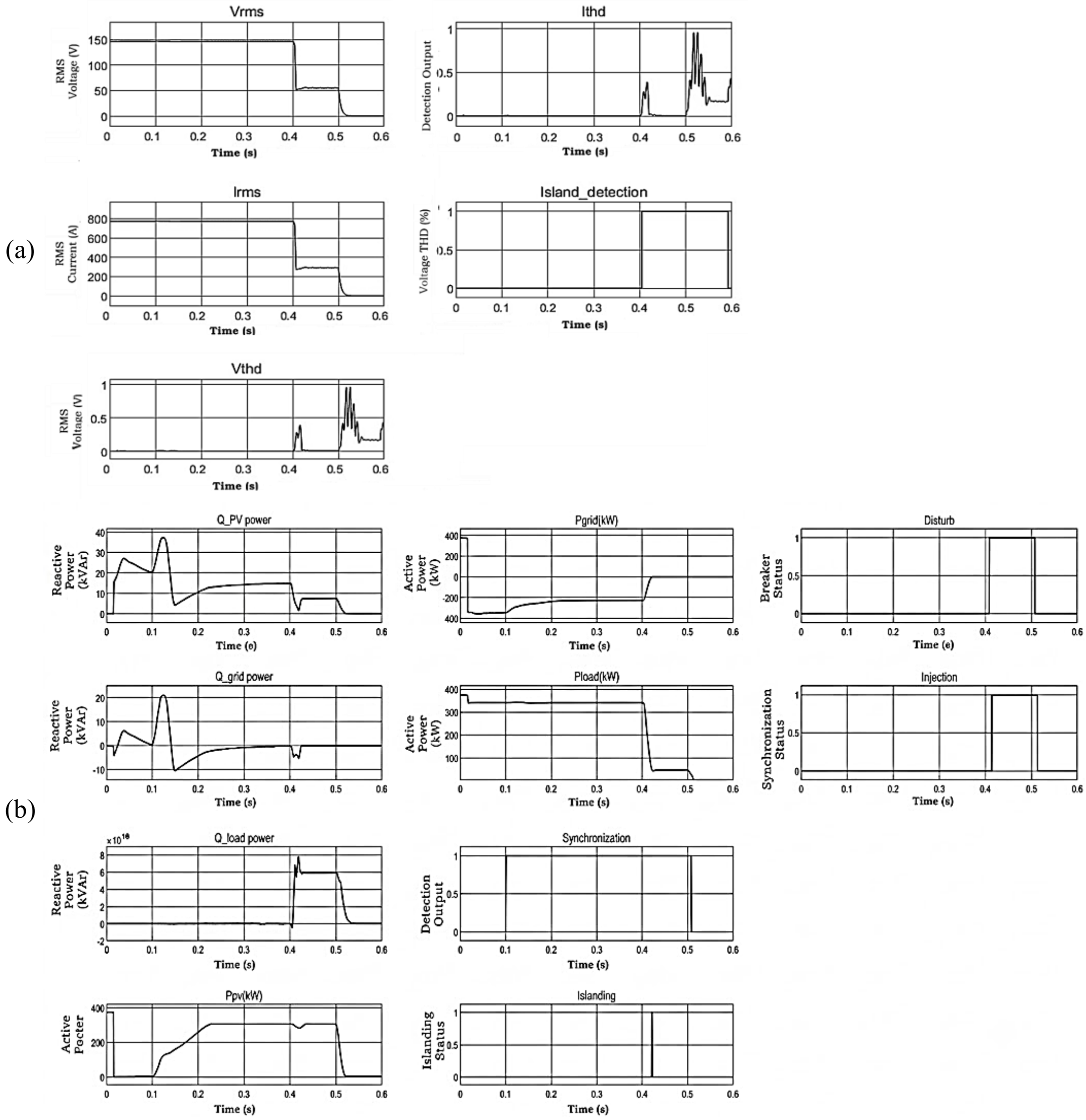

Figure 9. Simulation results under Cases 6 and 7: (a) system voltage and current responses with island detection in Case 6 and (b) DG–load power match in Case 7

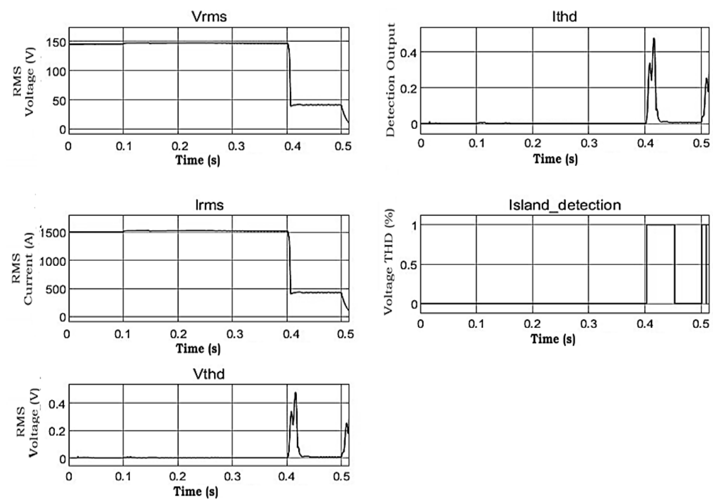

Figure 10. Voltage and current response of the system and island detection under Case 7

5. CONCLUSION

In this research, the critical problem of islanding detection in multi-source distribution generators is investigated. Islanding detection is important since it plays a critical role in ensuring the safety and stability of distributed energy systems. The proposed hybrid approach detects the islanding even in NDZ. This zone protects the DG system against false positives, thereby reducing the risk of unintentional islanding when islanding is not occurring. The proposed methodology has been tested under various loss-of-load conditions, demonstrating its robustness and effectiveness across different fault scenarios. The performance of the ANFIS based on the adaptive fuzzy classifier is compared with the conventional islanding detection technique, and the simulation results show that the proposed approach exhibits a superior performance in terms of detecting islanding faster compared to the conventional method. For future research, the proposed approach can be extended to design an islanding detection approach for resilient microgrids, which continues to supply power in the event of disruptions.

FUNDING INFORMATION

This research did not receive any specific grant from funding agencies in the public, commercial, or non-profit sectors.

AUTHOR CONTRIBUTIONS STATEMENT

This journal uses the Contributor Roles Taxonomy (CRediT) to recognize individual author contributions, reduce authorship disputes, and facilitate collaboration.

Name of Author	C	M	So	Va	Fo	I	R	D	O	E	Vi	Su	P	Fu
Madamaneri Ramya	✓	✓	✓	✓	✓	✓	✓	✓	✓	✓	✓		✓	✓
Thangellamudi Devaraju	✓	✓		✓	✓	✓	✓		✓	✓		✓		

C : **C**onceptualization
M : **M**ethodology
So : **So**ftware
Va : **Va**lidation
Fo : **Fo**rmal analysis
I : **I**nvestigation
R : **R**esources
D : **D**ata Curation
O : Writing - **O**riginal Draft
E : Writing - Review & **E**diting
Vi : **Vi**sualization
Su : **Su**pervision
P : **P**roject administration
Fu : **Fu**nding acquisition

CONFLICT OF INTEREST STATEMENT

The authors state no conflict of interest.

DATA AVAILABILITY

The data that support the findings of this study were generated using MATLAB/Simulink simulations of the proposed hybrid ANFIS and adaptive fuzzy classification framework for islanding detection. The simulation models, generated datasets, and supporting materials are available from the corresponding author upon reasonable request.

REFERENCES

[1] J. C. Gomez, J. Vaschetti, C. Coyos, and C. Ibarlucea, "Distributed generation: impact on protections and power quality," *IEEE Latin America Transactions*, vol. 11, no. 1, pp. 460–465, Feb. 2013, doi: 10.1109/TLA.2013.6502846.
[2] D. Çelik and M. E. Meral, "Current control based power management strategy for distributed power generation system," *Control Engineering Practice*, vol. 82, pp. 72–85, Jan. 2019, doi: 10.1016/j.conengprac.2018.09.025.
[3] E. Baneshi, H. Kolahduzloo, J. Ebrahimi, M. Mahmoudian, E. Pouresmaeil, and E. M. G. Rodrigues, "Coordinated power sharing in islanding microgrids for parallel distributed generations," *Electronics*, vol. 9, no. 11, Nov. 2020, doi: 10.3390/electronics9111927.
[4] B. Kumar Panigrahi, R. Nandi, B. Mahanta, and K. Pal, "Islanding detection in distributed generation," in *2016 International Conference on Circuit, Power and Computing Technologies (ICCPCT)*, Mar. 2016, pp. 1–5, doi: 10.1109/ICCPCT.2016.7530295.
[5] Y. A. Elshrief, S. Abd-Elhaleem, B. A. Abozalam, and A. D. Asham, "Methods for protecting network from islanding danger," *Journal of Engineering Research*, vol. 9, no. 2, pp. 171–183, Jun. 2021, doi: 10.36909/jer.v9i2.9695.
[6] Y. A. Elshrief, S. Abd-Elhaleem, B. Abo Zalam, and A. D. Asham, "On active anti-islanding techniques: survey," *Indonesian Journal of Electrical Engineering and Computer Science*, vol. 22, no. 2, pp. 609–618, May 2021, doi: 10.11591/ijeecs.v22.i2.pp609-618.
[7] Y. A. Elshrief, A. Danial, D. Helmi, and B. A. Abozalam, "On remote anti-islanding detection techniques- 3-2019," in *The Future of Electricity Grids: Challenges and Opportunities*, pp. 297–304, 2019.
[8] Y. A. Elshrief, D. H. Helmi, S. Abd-Elhaleem, B. A. Abozalam, and A. D. Asham, "Fast and accurate islanding detection technique for microgrid connected to photovoltaic system," *Journal of Radiation Research and Applied Sciences*, vol. 14, no. 1, pp. 210–221, Dec. 2021, doi: 10.1080/16878507.2021.1923913.

[9] Y. A. Elshrief, D. H. Helmi, A. D. Asham, and B. A. Abozalam, "Merits and demerits of the distributed generations connected to the utility grid," *Menoufia Journal of Electronic Engineering Research*, vol. 28, no. 1, pp. 259–262, Dec. 2019, doi: 10.21608/mjeer.2019.70907.
[10] B. Pancha, R. Shrestha, and A. K. Jha, "Islanding detection in distributed generation integrated thimi – Sallaghari distribution feeder using wavelet transform and artificial neural network," *Journal of the Institute of Engineering*, vol. 15, no. 2, pp. 55–61, Jul. 2019, doi: 10.3126/jie.v15i2.27641.
[11] S. S. Mohapatra, M. K. Maharana, A. Pradhan, P. K. Panigrahi, and R. C. Prusty, "Detection and diagnosis of islanding using artificial intelligence in distributed generation systems," *Sustainable Energy, Grids and Networks*, vol. 29, p. 100576, Mar. 2022, doi: 10.1016/j.segan.2021.100576.
[12] J. A. Cebollero, D. Cañete, S. Martín-Arroyo, M. García-Gracia, and H. Leite, "A survey of islanding detection methods for microgrids and assessment of non-detection zones in comparison with grid codes," *Energies*, vol. 15, no. 2, p. 460, Jan. 2022, doi: 10.3390/en15020460.
[13] N. A. Larik, M. F. Tahir, Z. M. S. Elbarbary, M. Z. Yousaf, and M. A. Khan, "A comprehensive literature review of conventional and modern islanding detection methods," *Energy Strategy Reviews*, vol. 44, p. 101007, Nov. 2022, doi: 10.1016/j.esr.2022.101007.
[14] U. Markovic, D. Chrysostomou, P. Aristidou, and G. Hug, "Impact of inverter-based generation on islanding detection schemes in distribution networks," *Electric Power Systems Research*, vol. 190, p. 106610, Jan. 2021, doi: 10.1016/j.epsr.2020.106610.
[15] S. Shrivastava, S. Jain, R. K. Nema, and V. Chaurasia, "Two level islanding detection method for distributed generators in distribution networks," *International Journal of Electrical Power & Energy Systems*, vol. 87, pp. 222–231, May 2017, doi: 10.1016/j.ijepes.2016.10.009.
[16] Y. M. Makwana and B. R. Bhalja, "Experimental performance of an islanding detection scheme based on modal components," *IEEE Transactions on Smart Grid*, vol. 10, no. 1, pp. 1025–1035, Jan. 2019, doi: 10.1109/TSG.2017.2757599.
[17] Q. Cui, K. El-Arroudi, and G. Joos, "Islanding detection of hybrid distributed generation under reduced non-detection zone," *IEEE Transactions on Smart Grid*, vol. 9, no. 5, pp. 5027–5037, Sep. 2018, doi: 10.1109/TSG.2017.2679101.
[18] T. S. Menezes, R. A. S. Fernandes, and D. V. Coury, "Intelligent islanding detection with grid topology adaptation and minimum non-detection zone," *Electric Power Systems Research*, vol. 187, p. 106470, Oct. 2020, doi: 10.1016/j.epsr.2020.106470.
[19] A. Serrano-Fontova, J. A. Martinez, P. Casals-Torrens, and R. Bosch, "A robust islanding detection method with zero-non-detection zone for distribution systems with DG," *International Journal of Electrical Power & Energy Systems*, vol. 133, p. 107247, Dec. 2021, doi: 10.1016/j.ijepes.2021.107247.
[20] S. Ramachandradurai, N. Krishnan, and N. Prabaharan, "Unintentional passive islanding detection and prevention method with reduced non-detection zones," *Energies*, vol. 15, no. 9, p. 3038, Apr. 2022, doi: 10.3390/en15093038.
[21] Y. A. Elshrief *et al.*, "An innovative hybrid method for islanding detection using fuzzy classifier for different circumstances including NDZ," *Journal of Radiation Research and Applied Sciences*, vol. 15, no. 2, pp. 129–142, Jun. 2022, doi: 10.1016/j.jrras.2022.04.008.
[22] M. Seyedi, S. A. Taher, B. Ganji, and J. Guerrero, "A hybrid islanding detection method based on the rates of changes in voltage and active power for the multi-inverter systems," *IEEE Transactions on Smart Grid*, vol. 12, no. 4, pp. 2800–2811, Jul. 2021, doi: 10.1109/TSG.2021.3061567.
[23] R. AbdelHady, "Modeling and simulation of a micro grid-connected solar PV system," *Water Science*, vol. 31, no. 1, pp. 1–10, Apr. 2017, doi: 10.1016/j.wsj.2017.04.001.
[24] L. Fara and D. Craciunescu, "Output analysis of stand-alone PV systems: modeling, simulation and control," *Energy Procedia*, vol. 112, pp. 595–605, Mar. 2017, doi: 10.1016/j.egypro.2017.03.1125.
[25] A. K. Ozcanli and M. Baysal, "Islanding detection in microgrid using deep learning based on 1D CNN and CNN-LSTM networks," *Sustainable Energy, Grids and Networks*, vol. 32, p. 100839, Dec. 2022, doi: 10.1016/j.segan.2022.100839.
[26] Y. M. Nsaif, M. S. Hossain Lipu, A. Hussain, A. Ayob, and Y. Yusof, "Island detection for grid connected photovoltaic distributed generations via integrated signal processing and machine learning approach," *International Journal of Electrical Power & Energy Systems*, vol. 154, p. 109468, Dec. 2023, doi: 10.1016/j.ijepes.2023.109468.

BIOGRAPHIES OF AUTHORS

Madamaneri Ramya is a research scholar in the Department of Electrical and Electronics Engineering, School of Engineering at Mohan Babu University (MBU). She is currently a lecturer in the Electrical and Electronics Engineering Section, Government Polytechnic, Chandragiri, Andhra Pradesh, India. She completed her B.Tech. and M.Tech. at Jawaharlal Nehru Technological University, Anantapur, India. Her main research includes islanding detection, adaptive learning, changes in demand, deep learning techniques, distributed energy resources, dynamic scheduling, energy consumption, energy cost, energy distribution, and energy management. She published two articles on her research area. She can be contacted at email: mullakurianusha@gmail.com.

Dr. Thangellamudi Devaraju is currently working as a professor in Department of Electrical and Electronics Engineering at School of Engineering, Mohan Babu University, Andhra Pradesh, India. His main research directions include convolutional voltage stability, power quality, neural networks (ANN), IoT, adaptive learning, analog-to-digital converter, authentication system, automated teller machines, automatic system, biometric authentication systems, biometric identification, biometric systems, biometric technologies, cybersecurity, DC-link capacitor, deep learning, deep learning techniques, digital signal processing, discrete fourier transform, distributed energy resources, distribution system, dynamic scheduling, energy management (consumption, cost, demand, distribution, energy supply, and sources), eye blinks, eye-tracking, face detection, face recognition, and facial features. He published over 100 articles on his research area. He can be contacted at email: haris.eee@gmail.com.